J|A|C|S ARTICLES

Published on Web 02/02/2010

Mixed Anion (Phosphate/Oxalate) Bonding to Iron(III) Materials

Fiona R. Kizewski,[†] Paul Boyle,[†] Dean Hesterberg,[‡] and James D. Martin*,[†]

Department of Chemistry, North Carolina State University, Raleigh, North Carolina 27695-8204, and Department of Soil Science, North Carolina State University, Raleigh, North Carolina 27695-7619

Received October 23, 2009; E-mail: jdmartin@ncsu.edu

Abstract: A novel phosphate/oxalate inorganic−organic hybrid material has been prepared to elucidate synthesis and bonding characteristics of iron(III) with both phosphate and organic matter (OM). Such mixed anion bonding of inorganic oxyanions and OM to iron(III) and aluminum(III) in environmental systems has been proposed but not proven, mainly because of the complexity of natural geochemical matrices. The compound reported here with the molecular formula of $[C_3H_{12}N_2]_2[Fe_5(C_2O_4)_2(H_xPO_4)_8]$ (**I**) was hydrothermally synthesized and characterized by single crystal X-ray diffraction and X-ray absorption spectroscopy (XAS). In this new structure, Fe−O octahedra and P−O tetrahedra are connected by corner-sharing to form a 2-D network in the *a*−*b* plane. Oxalate anions cross-link these Fe−P layers constructing a 3-D anionic framework. A diprotonated structure-directing template, DAP (1,3-diaminopropane), resides in the oxalate layer of the structure and offsets the negative charge of the anionic framework. Iron K-edge XANES spectra confirmed that the iron in **I** is Fe(III). The crystal structure of **I** is used to successfully fit its Fe K-edge EXAFS spectrum, which exhibits spectral signatures that unambiguously identify iron-phosphate and iron-OM bonding. Such molecular spectroscopic features will be invaluable for the evaluation of complex environmental systems. Furthermore, syntheses demonstrated the critical role of the templating amine to mediate whether or not the iron(III) is reduced by the organic acid.

Introduction

Chemical speciation (chemical form) of contaminants largely controls their mobility and potential toxicity in environmental systems including the soil-subsurface continuum, groundwater aquifers, freshwater, and marine sediments. However, characterization of contaminant speciation is hindered by the extreme complexity of these systems. Contaminants like phosphate, arsenate, and metal cations can be bonded to multiple matrix components that include various oxide, hydroxide, and silicate minerals and structurally heterogeneous organic matter (humics), as well as ternary adducts of these components.[1] Moreover, adsorbed, mineral, and coprecipitated forms of contaminants can coexist in nature, presenting an analytical challenge for characterizing chemical speciation.

Although phosphorus is an essential macronutrient for life, excessive P inputs from agricultural systems is a major environmental concern because P transfer to surface waters causes eutrophication. Understanding mechanisms for P binding in soils, sediment, or other natural geochemical systems is extremely important to predict P distribution and mobility. Phosphate concentration, matrix composition (e.g., mineralogy and OM content), pH, and redox properties are considered primary determining factors in controlling phosphate binding and mobility in both soils and sediments.[2−5] These matrices are complex, multicomponent materials, with sorbed or mineral precipitated inorganic phosphate being a relatively minor component. Thus, characterizing the fundamental characteristics of phosphate binding to minerals is challenging, particularly in the presence of organic matter (OM). Iron and aluminum oxide minerals are considered important sorbents for phosphate in acid soils.[6,7] Moreover, it has been hypothesized that natural organic matter significantly impacts phosphate sorption via the formation of OM-Fe(III)-PO_4 or OM-Al(III)-PO_4 ternary complexes, though direct evidence for such ternary complexation is lacking.[8−10]

Spectroscopic methods for directly characterizing molecular bonding in environmental systems are usually compromised by interfering elements or the extreme complexity of the matrix. For example, nuclear magnetic resonance (NMR) spectroscopy suffers from interference by the magnetism of Fe, one of the more abundant elements in earth-surface systems. Fourier-transform infrared (FT-IR) spectroscopy analysis of minor

[†] Department of Chemistry.
[‡] Department of Soil Science.

(1) Brown, G. E.; Sturchio, N. C. *Appl. Sync. Rad. LT Geochem. Env. Sci.* **2002**, *49*, 1–115.
(2) Banerjee, S. K.; Sengupta, M.; Gupta, S. K. *J. Ind. Chem. Soc.* **1980**, *57* (2), 188–190.
(3) Bhatti, J. S.; Comerford, N. B.; Johnston, C. T. *Soil Sci. Soc. Am. J.* **1998**, *62* (4), 1089–1095.
(4) Antelo, J.; Arce, F.; Avena, M.; Fiol, S.; Lopez, R.; Macias, F. *Geoderma* **2007**, *138* (1−2), 12–19, Kq.
(5) Skoog, A.; Arias-Esquivel, V. A. *Geochim. Cosmochim. Acta* **2008**, *72* (12), A874–A874.
(6) Violante, A.; Pigna, M. *Soil Sci. Soc. Am. J.* **2002**, *66* (6), 1788–1796.
(7) Khare, N.; Martin, J. D.; Hesterberg, D. *Geochim. Cosmochim. Acta* **2007**, *71*, 4405–4415.
(8) Bloom, P. R. *Soil Sci. Soc. Am. J.* **1981**, *45* (2), 267–272.
(9) Gerke, J.; Hermann, R. *Z. Pflanzenernah. Bodenkd.* **1992**, *155* (3), 233–236.
(10) Gerke, J. *Geoderma* **1993**, *59* (1−4), 279–288.

components like phosphate in environmental samples is often hindered by stronger, overlapping absorption bands of more dominant matrix components. X-ray absorption spectroscopy is an element-specific technique that is less subject to matrix interferences than other spectroscopies. But the resulting spectrum reflects the average local molecular coordination environment around atoms of the absorber element. Hence, in complex matrices, XAS does not directly distinguish, for example, between ternary coordination structures involving an inorganic oxyanion and an organic ligand bonded to the same metal center versus a mixture of binary complexes of each of these ligands to different metal centers. It is therefore necessary to obtain structurally well-defined systems that can be used as models for spectroscopically interrogating more complex systems.

A search of the Cambridge Crystallographic Database for structures containing small-molecule organic acids that would serve as OM analogues reveals very few phosphate-Fe(III)-organic-acid ternary complexes, with the majority of known crystal structures being phosphate-Fe-oxalate complexes.[11−15] Among these phosphate/oxalate containing materials, virtually all of the syntheses require the presence of an amine, even in the reported structure in which no amine is found in the hybrid framework.[16] The fact that few pure ternary crystalline structures exist raises additional questions as to the compatibility of organic acid and phosphate anions binding to the same metal center.

X-ray absorption near edge structure (XANES) spectroscopy at the phosphorus K-edge has recently been exploited to probe phosphate binding in environmental matrices.[17−19] By comparing spectra from these systems with minerals of known structure, it was shown that P K-edge XANES can effectively differentiate phosphate bound to iron and aluminum oxide minerals based on the characteristics of prewhite line features.[20,21] In addition, researchers have applied iron K-edge EXAFS (extended X-ray absorption fine structure) to investigate the Fe coordination environment in soil organic matter.[22−24] Using Fe EXAFS, Karlsson et al.[25] proposed that Fe either exists as mononuclear Fe(III)-OM complexes or precipitated as Fe(III) (hydr)oxides. However, no literature to date provides conclusive experimental evidence for the hypothesized PO_4-Fe-OM ternary complexation.

Thus the aim of this research was to synthesize and characterize a crystalline ternary compound, specifically involving phosphate and a carboxylic acid bound to a common iron(III) center, that would serve as a model system for XAS spectroscopic interrogation of ternary complexation in natural systems.

From a series of syntheses attempting to reproduce bulk quantities of template free iron phosphate/oxalate materials that were reported in the literature,[16] a new templated iron phosphate/oxalate material was discovered. We here report the synthesis, single crystal structural, and XAS characterization of $[DAP]_2[Fe_5(C_2O_4)_2(H_xPO_4)_8]$ (**I**) (DAP = $C_3H_{12}N_2$). While the gross framework bonding is similar among all of the reported iron(III) phosphate/oxalate materials,[11−16] **I** represents the most phosphate rich (P/Fe = 1.6) and the second most oxalate poor (Ox/Fe = 0.4) of these materials. In this study, a combination of the precise structural detail from the single crystal structure with thorough XAS spectroscopic characterization that is amenable to bulk and trace material analysis demonstrates an important application of fundamental structural chemistry for the development of a molecular understanding of complex environmental systems.

Results

Synthesis of $[DAP]_2[Fe_5(C_2O_4)_2(H_xPO_4)_8]$, I. In keeping with literature reports of mixed anion (phosphate/organic acid) materials,[16] reactions were explored both with and without the addition of potentially structure directing amines as templates. Hydrothermal treatment of an aqueous solution of H_3PO_4, 1,3-diaminopropane (DAP), $FeCl_3 \cdot 6H_2O$, and $H_2C_2O_4$ (see experimental) yielded a pale pink crystalline product. Single crystals were harvested for X-ray diffraction analysis, and X-ray powder diffraction confirmed that the bulk product was the same material as the single crystal. Thermogravimetric analysis of **I** from room temperature to 800 °C under a N_2 atmosphere exhibited a sharp weight loss of 23% starting approximately at 300 °C followed by two more gradual weight loss steps of an additional 6% (see Supporting Information Figure S1). This result is consistent with an initial decomposition resulting in the loss of the templating ammonium cation and the carboxylate ligands, calculated to be 23.8% based on the chemical formula determined from the single crystal structure. The subsequent 6% weight loss is consistent with the loss of 4.5 equiv of water (calculated = 5.9%) from decomposition of the HPO_4^{2-} and $H_2PO_4^-$ ligands, for which there are 9 protons per formula unit, likely forming pyrophosphate ligands upon loss of water.

Interestingly, the order of addition of the reactants is critical in obtaining a significant yield of **I**. To obtain the highest yield of **I**, the amine, DAP, is added to the phosphoric acid solution, followed by the iron chloride and finally the oxalic acid. By contrast, when DAP is added as the final reactant, a pale green solution is achieved after addition of H_3PO_4, $FeCl_3 \cdot 6H_2O$, and $H_2C_2O_4$. Subsequent addition of the amine yields a colorless precipitate resulting in a slurry that does not redissolve after 30 min of stirring at room temperature. After hydrothermal treatment of this slurry, the major product is a black crystalline material. This material was identified as $Fe_3(PO_4)_2(OH)_2$ by powder X-ray diffraction. Reactions performed in the absence of the added amine similarly formed $Fe(PO_4)_2(OH)_2$.

Single Crystal Structure. The crystal structure of **I** was determined by single crystal X-ray diffraction; a summary of the crystallographic data is given in Table 1. Full details of the structure solution are available in the Supporting Information. An ORTEP drawing of the asymmetric unit of **I** is given in

(11) Choudhury, A.; Natarajan, S.; Rao, C. N. R. *Chem. Mater.* **1999**, *11* (9), 2316–2318.
(12) Lin, H. M.; Lii, K. H.; Jiang, Y. C.; Wang, S. L. *Chem. Mater.* **1999**, *11* (3), 519–521.
(13) Choudhury, A.; Natarajan, S. *J. Mater. Chem.* **1999**, *9* (12), 3113–3117.
(14) Chang, W. J.; Lin, H. M.; Lii, K. H. *J. Solid State Chem.* **2001**, *157* (1), 233–239.
(15) Jiang, Y. C.; Wang, S. L.; Lii, K. H.; Nguyen, N.; Ducouret, A. *Chem. Mater.* **2003**, *15* (8), 1633–1638.
(16) Choudhury, A.; Natarajan, S.; Rao, C. N. R. *Chem.—Eur. J.* **2000**, *6* (7), 1168–1175.
(17) Beauchemin, S.; Hesterberg, D.; Chou, J.; Beauchemin, M.; Simard, R. R.; Sayers, D. E. *J. Env. Qual.* **2003**, *32* (5), 1809–1819.
(18) Kruse, J.; Leinweber, P. *J. Plant Nut. Soil Sci.* **2008**, *171* (4), 613–620.
(19) Seiter, J. M.; Staats-Borda, K. E.; Ginder-Vogel, M.; Sparks, D. L. *J. Env. Qual.* **2008**, *37* (2), 477–485.
(20) Khare, N.; Hesterberg, D.; Beauchemin, S.; Wang, S. L. *Soil Sci. Soc. Am. J.* **2004**, *68* (2), 460–469.
(21) Khare, N.; Hesterberg, D.; Martin, J. D. *Environ. Sci. Technol.* **2005**, *39* (7), 2152–2160.
(22) Vilge-Ritter, A.; Rose, J.; Masion, A.; Bottero, J. Y.; Laine, J. M. *Colloids Surf., A* **1999**, *147* (3), 297–308.
(23) Gustafsson, J. P.; Persson, I.; Kleja, D. B.; Van Schaik, J. W. J. *Environ. Sci. Technol.* **2007**, *41* (4), 1232–1237.
(24) van Schaik, J. W. J.; Persson, I.; Kleja, D. B.; Gustafsson, J. P. *Environ. Sci. Technol.* **2008**, *42* (7), 2367–2373.
(25) Karlsson, T.; Persson, P.; Skyllberg, U.; Morth, C. M.; Giesler, R. *Environ. Sci. Technol.* **2008**, *42* (15), 5449–5454.

Table 1. Crystal Data and Structure Refinement Parameters of **I**

Empirical formula	$[C_6H_{24}N_4][C_4H_9O_{40}P_8Fe_5]$
Formula weight	1376
Crystal Dimensions (mm^3)	0.10 × 0.08 × 0.05
Crystal Color and Habit	colorless prism
Crystal System	triclinic
Space Group	$P\bar{1}$
Temperature, K	173
a, Å	9.7851(3)
b, Å	9.8986(3)
c, Å	10.7420(3)
α, deg	73.7900(15)
β, deg	71.6838(14)
γ, deg	79.3001(13)
V, $Å^3$	942.99(5)
Z	1
R^a	0.037
$R_w{}^b$	0.051
GOF	1.48

[a] $R = \Sigma||F_o| - |F_c||/\Sigma|F_o|$. [b] $R_w = \Sigma(|F_o| - |F_c|)^2/\Sigma|F_o|^2$.

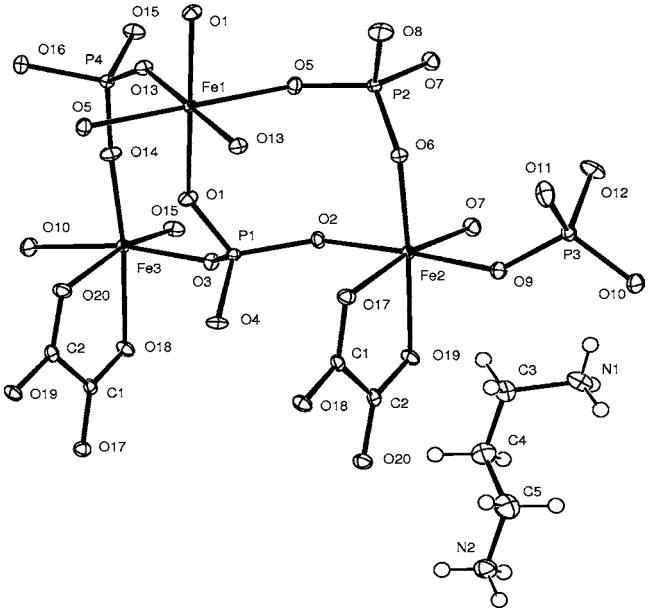

Figure 1. ORTEP drawing of the asymmetric unit of **1** which describes the atom labeling scheme.

Table 2. P−O Bond Lengths in **I**

P	O	Length (Å)	Bound to
P1	O1	1.525(2)	Fe1
	O2	1.538(2)	Fe2
	O3	1.534(2)	Fe3
	O4	1.546(2)	terminal
P2	O5	1.520(2)	Fe1
	O6	1.535(2)	Fe2
	O7	1.499(2)	Fe2
	O8	1.590(2)	terminal
P3	O9	1.497(2)	Fe2
	O10	1.499(2)	Fe3
	O11	1.572(2)	terminal
	O12	1.572(2)	terminal
P4	O13	1.517(2)	Fe1
	O14	1.504(2)	Fe3
	O15	1.518(2)	Fe3
	O16	1.597(2)	terminal

Figure 1. The P−O and Fe−O distances are given in Tables 2 and 3. In the structure solution, only the heavy atom positions could be located in the difference maps. While the hydrogen

Table 3. Fe−O Bond Lengths and Bond Valence in **I**[a]

Fe	O	Distance (Å)	Bound to	Bond Valence
	O1	1.937(2)	P1	0.59
	O1	1.937(2)	P1	0.59
	O5	2.073(2)	P2	0.41
Fe1	O5	2.073(2)	P2	0.41
	O13	2.011(2)	P4	0.49
	O13	2.011(2)	P4	0.49
				2.98
	O2	1.929(2)	P1	0.61
	O6	1.999(2)	P2	0.50
	O7	1.923(2)	P2	0.62
Fe2	O9	1.974(2)	P3	0.54
	O17	2.095(2)	C	0.39
	O19	2.092(2)	C	0.39
				3.05
	O3	1.938(2)	P1	0.59
	O10	1.987(2)	P3	0.52
	O14	1.923(2)	P4	0.62
Fe3	O15	1.915(2)	P4	0.63
	O18	2.137(2)	C	0.35
	O20	2.111(2)	C	0.37
				3.08

[a] Bond valence calculated as $v_i = \exp((R_0 - R)/b)$ where $R_0 = 1.744$ and $b = 0.37$.

atoms associated with the DAP cation can be reasonably placed in calculated positions, the number of protons associated with the phosphate anions, let alone their positions, cannot be assigned without further analysis of the oxidation state of iron. The assignment of hydrogen phosphate protons can be accounted for by consideration of the O−P and O−Fe bonding, as will be described below. Symmetry independent iron atoms Fe2 and Fe3, which amount to 4/5 of the total iron atoms, are ligated to both oxalate and phosphate anions, whereas Fe1 is only ligated to phosphate. In all cases the phosphate anions are bound in an η^1-fashion to the metal centers, with P1, P2, and P4 each bound to three distinct iron atoms and P3 bridging only two kinds of iron atoms. The corresponding terminal P−O bonds are the most likely locations of H atoms of the hydrogen- or dihydrogen-phosphate ligands.

In this structure, moieties of FeO_6, PO_4, and C_2O_4 are assembled into a 3-D anionic framework, which is charge balanced and templated by DAP alkylammonium cations. A series of views of the crystal packing are given in Figure 2. A distinguishing feature to help visualize this structure is the chains running along the ⟨−1,−1,3⟩ direction consisting of iron octahedra (Fe2 and Fe3) for which opposite edges are alternately bridged by either a pair of phosphates (a pair of P2 or a pair of P4) or a single oxalate ligand. These chains are distributed in approximately a square grid, most clearly seen in the projections of Figure 2c and d and are pairwise connected along the ⟨1,−1,0⟩ direction by another phosphate bridge (P1 or P3). In three dimensions, the Fe2 and Fe3 octahedra are distributed in a distorted CsCl-type packing with one-quarter of the distorted CsCl-type cubes centered by an Fe1 octahedron, one-quarter of the distorted cubes empty, and half centered by DAP cations. Stacked together, these result in the large cation filled cage shown in Figure 2b.

Alternatively, it can be useful to view the structure of **I** as being composed of alternating organic and inorganic layers, parallel to the (001) plane, as highlighted with green and purple brackets, respectively in Figure 2a. The organic layers contain the $C_2O_4^{2-}$ ligands and DAP cations, whereas the inorganic layers exclusively contain iron phosphate. These respective inorganic and organic layers are shown in Figure 2c and d, as

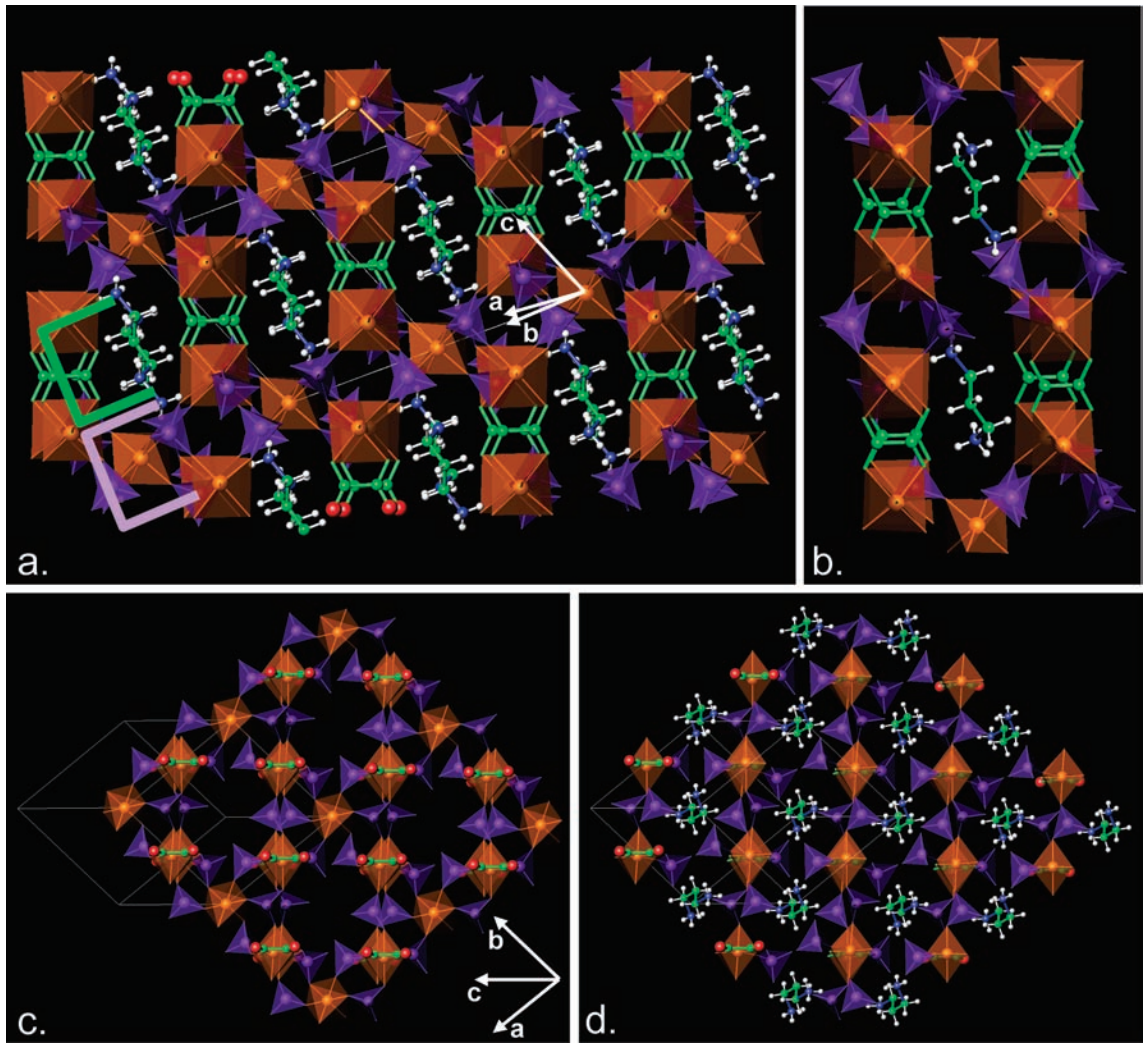

Figure 2. (a) Crystal packing view of the structure of **I** oriented to emphasize the phosphate/oxylate chains that run along the ⟨−1, −1, 3⟩ direction (vertical in figure). Green and purple brackets emphasize the (0,0,2) alternating iron phosphate and iron oxalate layers of the structure. (b) View of the phosphate/oxalate cage templated by two DAP cations. View of the (c) iron phosphate and (d) iron oxalate layers as viewed looking down the ⟨−1,−1,3⟩ direction. The alkylammonium cations reside within the oxalate layers.

projected onto the (−1−13) plane, the direction which is approximately perpendicular to the iron phosphate/oxalate chains described above. Again it can be seen that the Fe1 octahedra and the DAP cations fill comparative sites, the former bridged by phosphates and the latter sitting in an oxalate cage with the ammonium head groups hydrogen bonded to the phosphates above and below the organic layer.

X-ray Absorption Spectroscopy. The X-ray absorption spectrum of **I** was collected at the Fe K-edge, and the XANES portion was compared with that of $FePO_4 \cdot 2H_2O$ (strengite), an Fe(III) standard; $Fe_3(PO_4)_2 \cdot 8H_2O$, an Fe(II) standard; and iron foil, an Fe(0) standard. The EXAFS portion of these spectra is discussed in a later section. XANES spectra are given in Figure 3 for **I** and the comparative standards, and the derivative XANES spectra for **I** and strengite are given in Figure 4. The pre-edge peak observed in the spectrum at ∼7113 eV has been assigned to the electronic transition from the Fe-1s core orbital to the Fe-3d based M-L σ^* antibonding molecular orbital.[26] The more prominent features of the absorption edge at approximately 7125 and 7128 eV can be assigned to the electronic transition from the Fe-1s core to the Fe4p-O2p σ^* and the P3p-O2p σ^* antibonding molecular orbitals.[7] The energy of these transitions, noted by the inflection points of the pre-edge and edge features

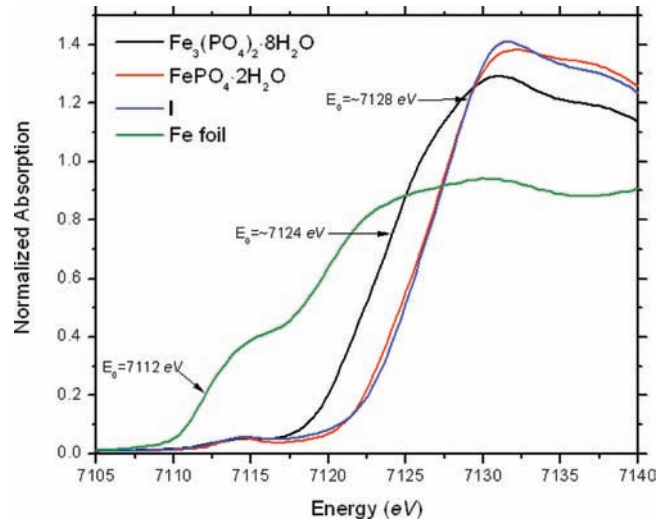

Figure 3. Normalized Fe K-edge XANES spectrum of **I** (blue), compared with the spectra of the Fe(III) standard strengite ($FePO_4 \cdot 2H_2O$) (red), the Fe (II) standard $Fe_3(PO_4)_2 \cdot 8H_2O$ (black), and iron foil (green).

(26) Grunes, L. A. *Phys. Rev. B* **1983**, *27* (4), 2111–2131.

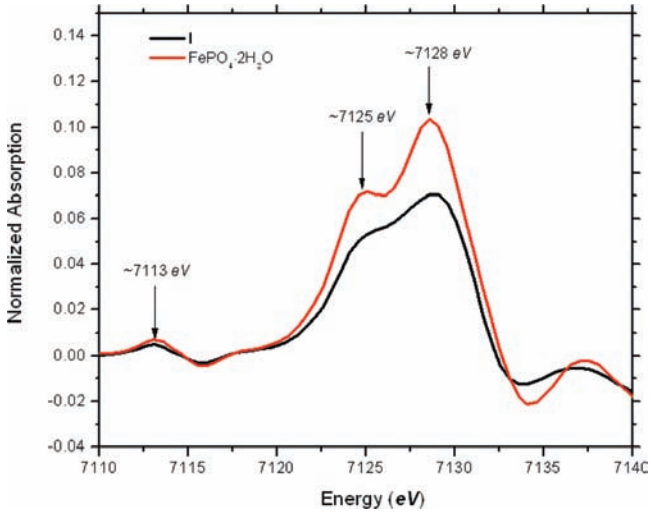

Figure 4. First derivative spectra of the Fe K-edge XANES of **I** (black) and strengite ($FePO_4 \cdot 2H_2O$) (red).

(most easily seen as peaks in the derivative spectra in Figure 4), is highly sensitive to the oxidation state of Fe; the stronger Fe−O bonding in an Fe(III) environment shifts this transition to higher energy. The XANES spectra show little difference between that of **I** and strengite, both of which exhibit transitions at significantly higher energy than is observed for the Fe(II) and Fe(0) standards. Therefore, it can be reasonably inferred that all Fe atoms in **I** have the same oxidation state of those in strengite, i.e. Fe(III). This is also consistent with the oxidation state assignment based on bond valence sums calculated from the Fe−O distances, Table 3.

Discussion

Synthesis of Mixed Anion Materials. We have successfully prepared a new iron(III) phosphate/oxalate material that, in addition to being a novel hybrid inorganic/organic framework, can serve as a useful model for analyzing structural details of possible phosphate/organic matter binding to iron in complex environmental matrices. A search of the Cambridge Crystallographic Database finds a relatively small number of iron(III) mixed phosphate/organic acid materials, with those reported being exclusively with oxalate as the organic acid anion. Furthermore, almost all of the mixed anion compounds reported exhibit a framework structure that is templated by an organic ammonium cation. This in part is likely due to the fact that many organic acids can reduce Fe(III) to Fe(II). The standard reduction potentials for Fe(III)/Fe(II) exhibit considerable variation depending on the anionic species present. For example, the CRC Handbook of Chemistry and Physics reports the standard Fe(III)/Fe(II) reduction potential to be 0.77 V in 1f HCl, but 0.44 V in 1f H_3PO_4. Given the standard reduction potential of oxalic acid is −0.49 V, it is not surprising that the extent of iron reduction in the presence of an organic acid will be very dependent on synthesis conditions. Because the reduction of Fe(III) by oxalate is known to be photosensitive,[27,28] reactions were carried out in the dark. However, the synthetic variable found to have the greatest impact on the respective formation of the ternary compound **I** vs the reduction of iron and the resultant formation of $Fe_3(PO_4)_2(OH)_2$ was the sequential order in which the reactants were added. Reduction occurred when oxalic acid was added to a solution of H_3PO_4 and $FeCl_3$. By contrast, if the amine (DAP) was added to the reaction mixture prior to the addition of the oxalic acid, no iron reduction was observed. These synthetic results suggest that the amine plays a significant role in preventing iron reduction by oxalate.

PO_4^{3-}, HPO_4^{2-}, or $H_2PO_4^{-}$. The Fe K-edge XANES spectra provide strong evidence that all of the iron in **I** exists in the +3 oxidation state. Given the heavy atom structure, discernible from the single crystal X-ray diffraction, for which the empirical formula includes two DAP cations, five iron atoms, and two oxalate and eight phosphate ligands, the phosphates must exist as some combination of nonprotonated phosphate, hydrogen phosphate, and/or dihydrogen phosphate ligands. To achieve charge neutrality a total of nine protons must be distributed among the eight phosphate ligands. An analysis of the P−O and Fe−O bond lengths, listed in Tables 2 and 3, affords a reasonable basis for P−O vs P−OH assignments. Clearly a terminal P═O double bond should exhibit the shortest distance. Given that H has a slightly greater electronegativity than Fe, the P−O distance is expected to be lengthened slightly when bridged to an H compared to when it is bridged to Fe. A bridging hydroxyl (P−OH−Fe) would be expected to also exhibit P−O elongation. Such a bridging hydroxyl would similarly be anticipated to exhibit a longer Fe−O distance than a nonprotonated Fe−O−P bridge. Known crystal structures bear out these expected trends.[29−31] By way of reference, the structure of $Fe(H_2PO_4)_3$ demonstrates that the bridging $P-O_{Fe}$ distance is 1.48 Å, while $P-O_H$ distances as long as 1.63 Å are observed,[31] whereas in $FePO_4 \cdot 2H_2O$ all the P−O bonds are bridged between Fe and P and exhibit distances within the narrow range of 1.52 to 1.54 Å.[29]

In **I**, P−O bond lengths are observed to range between 1.50 and 1.60 Å. With the exception of the terminal P1−O4 bond, the terminal P−O bonds are significantly longer (>0.06 Å) than the bridging P−O bonds suggesting that the terminal oxygens bound to P2, P3, and P4 each have protons bonded. Such P−O bond distance arguments account for a total of eight protons, one associated with each of the two P2 and P4 phosphates (hydrogen phosphate), and two associated with each of the two P3 phosphates (dihydrogen phosphate). Assignment of the ninth proton is less clear. While the terminal P1−O4 is the longest bond to P1, it is only 0.008 Å longer than the next longest bridging contact. Furthermore, O4 forms the closest contact to the alkylammonium cation. Thus hydrogen bonding to the ammonium template rather than being a hydrogen phosphate is the likely cause for the slight lengthening of the P1−O4 bond. Phosphate P1 therefore is assigned as a nonprotonated PO_4^{3-} ligand. Consideration of the Fe−O bonding finds that Fe1−O5 bonds (2.07 Å) are the longest $Fe-O_P$ bonds by more than 0.07 Å. Their neighbor Fe2−O6 is the next longest at 2.00 Å. Both O5 and O6 are bound to P2. It therefore is proposed that the ninth proton is associated with the P2 phosphate ligand. However, since each of the phosphate ligands exists as symmetry equivalent pairs because of a crystallographic inversion center, we suggest that P2 represents a mixed hydrogen phosphate/dihydrogen phosphate ligand. Overall then, these

(27) Siffert, C.; Sulzberger, B. *Langmuir* **1991**, *7* (8), 1627–1634.
(28) Goldberg, M. C.; Cunningham, K. M.; Weiner, E. R. *J. Photochem.Photobiol. A* **1993**, *73* (2), 105–120.
(29) Taxer, K.; Bard, H. *Cryst. Res. Technol.* **2004**, *39* (12), 1080–1088.
(30) Baies, R.; Pralong, V.; Caignaert, V.; Raveau, B. *Mater. Res. Bull.* **2006**, *41* (6), 1170–1177.
(31) Vencato, I.; Mascarenhas, Y. P.; Mattievich, E. *Am. Mineral.* **1986**, *71* (1−2), 222–226.

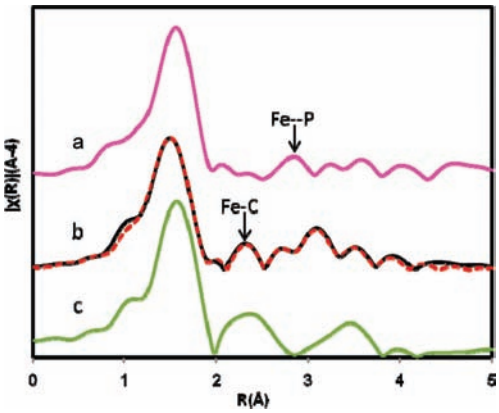

Figure 5. Fourier-transform magnitude of the Fe EXAFS spectrum of (a) strengite ($FePO_4 \cdot 2H_2O$), (b) **I**, and (c) $Fe_2(C_2O_4)_3 \cdot 6H_2O$. For (b) the solid line represents the experimental data, and the dotted line represents the calculated best fit using the single crystal structure as a model. Arrows highlight the Fe−P and Fe−C second nearest neighbor peaks in strengite and $Fe_2(C_2O_4)_3 \cdot 6H_2O$, respectively. (Distances are not corrected for phase shift.)

account for the empirical molecular formula of **I** being $[C_3N_2H_{12}]_2[Fe_5(C_2O_4)_2(H_2PO_4)_2(H_{1.5}PO_4)_2(HPO_4)_2(PO_4)_2]$.

Differentiation of Phosphate vs Organic Matter Binding by EXAFS. Examination of the structure of **I** as well as the structures of other Fe(III) materials with phosphate or organic acid (primarily oxalate or acetate) ligation demonstrates that while the metal−oxygen distances of these two ligand systems are reasonably similar (∼2.0 ± 0.1 Å), the second nearest neighbor distances between the iron and the phosphorus or carbon differ considerably (Fe−P ≈ 3.3 ± 0.1 Å and Fe−C ≈ 2.9 ± 0.1 Å). This difference should be well resolvable by EXAFS, a technique that is also amenable to characterization of complex environmental systems. The Fourier-transform magnitude of the k^3-weighted, Fe K-edge EXAFS spectrum of **I** along with the spectra of strengite ($FePO_4 \cdot 2H_2O$) and $Fe_2(C_2O_4)_3 \cdot 6H_2O$ and a fitting model based on the crystal structure of **I** are presented in Figure 5. Using the crystal structure of **I**, the contributions of signals from single- and multiple-scattering paths used to fit the spectrum can be evaluated as shown in Figure 6 with fitting parameters given in Table 4. The spectra of the strengite and iron oxalate controls (Figure 5a and c) clearly show the distinction between the

Table 4. Fitting Results of **I**, including Coordination Number (CN, Fixed), Interatomic Distance (R), and Debye−Waller Factors (S^2); Amplitude Reduction Factor (So^2) and delE° Apply to All Paths with So^2 Fixed at 0.84

Path	CN	R (Å)	δ^2
$Fe-O_P$[a]	4.67	1.9572 (0.0007)	0.005 (0.001)
$Fe-O_C$[a]	1.33	2.0926 (0.0007)	0.003 (0.001)
Fe−C	2	2.858 (0.005)	0.002 (0.001)
Fe−C−O	4	3.066 (0.002)	0.004 (0.009)
Fe−P	3	3.211 (0.001)	0.004 (0.001)
Fe−P−O	8	3.439 (0.005)	0.01 (0.005)
Fe−P	1	3.375 (0.002)	0.004 (0.002)
Fe−O−P−O	1	3.56 (0.02)	0.010 (0.003)
Fe−O	2	3.661 (0.002)	0.001 (0.002)
Fe−O−O	6	3.956 (0.002)	0.002 (0.009)
Fe−O + Fe−O	6	3.961 (0.002)	0.002 (0.009)
Fe−O−C	4	4.053 (0.002)	0.006 (0.006)
Fe−C−O−C	2	4.061 (0.002)	0.006 (0.006)
Fe−C−O−O	4	4.177 (0.002)	0.006 (0.006)
Fe−O−O	4	4.286 (0.002)	0.013 (0.010)
delE°		−0.72 (0.09)	
So^2		0.84 (fixed)	

[a] Subscripts denote O atoms from PO_4^{3-} or $C_2O_4^{2-}$ group, respectively. (Numbers in parentheses are calculated uncertainties).

phosphorus and carbon second nearest neighbors with a respective peak or lack of a peak in the R-space EXAFS spectrum corresponding to the respective Fe−C and Fe−P distances. In the R-space EXAFS spectrum of **I**, evidence of iron coordination to both oxalate and the phosphate is clearly present with the Fe−C and Fe−P signals between 2.2 and 3.0 Å (uncorrected) as shown in Figure 6. Clearly, the structural characteristics of **I** are well reflected in its EXAFS spectrum which thus provides an important fingerprint to differentiate phosphate from organic matter binding in complex natural systems.

Conclusions

A new iron phosphate/oxalate material has been prepared and characterized such that it provides a useful molecular level model to advance the understanding of phosphate binding in complex environmental systems. The reaction conditions necessary to form this mixed anion species demonstrate the significant role that the ligands and reaction medium have on controlling the redox state of the iron. Specifically in this system it is demonstrated that the alkylamine can prevent the organic acid from reducing the metal center and serve as a structure

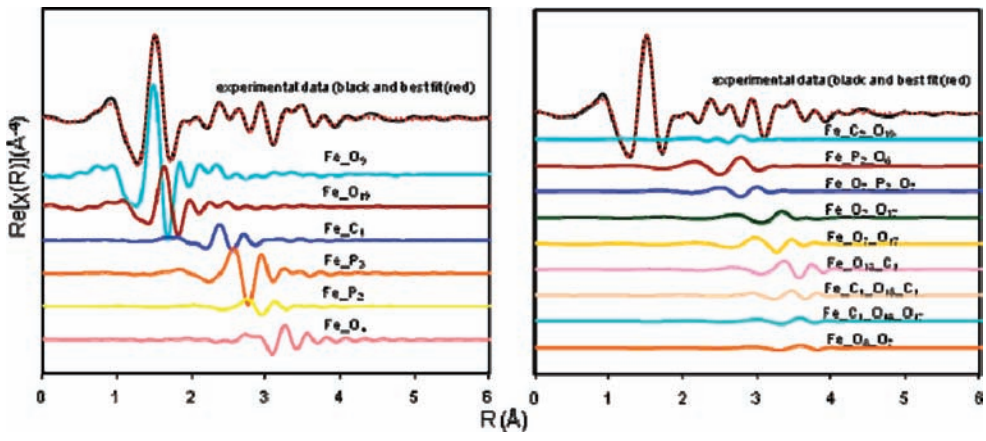

Figure 6. Fourier transform of the real part of the k^3-weighted Fe EXAFS spectrum of **I** (black) along with the best fit (red). The contributions of the signals from single-scattering paths (left) and multiple-scattering paths (right) calculated from the crystal structure of **I** (plotted in the lower portion of the figure with a different color assigned to each path) demonstrate the differential contribution of the iron to oxygen, phosphorus, and carbon neighbors. (Distances are not corrected for phase shift.)

directing template. Structurally, this new iron oxalate phosphate $[DAP]_2[Fe_5(C_2O_4)_2(H_2PO_4)_2(H_{1.5}PO_4)_2(HPO_4)_2(PO_4)_2]$, **I**, can conveniently be viewed as a hybrid structure of an alkylammonium templated organic layer, representative of a carboxylic acid structural network in natural OM, and an iron phosphate inorganic layer, representative of a mineral phosphate. Atomic structural parameters determined for **I**, as well as those from other ferric iron oxalatophosphate species,[11−16] indicate a measurable difference between Fe−P and Fe−C second coordination shell distances. In the characterization of **I** by both single crystal X-ray diffraction and X-ray absorption spectroscopy, we clearly demonstrate that EXAFS effectively can differentiate these. While real environmental systems are anticipated to be significantly more complex than this pure material, if ferric iron in a natural system is bound to both carboxyl groups from organic matter and phosphate, it should exhibit both Fe−C and Fe−P second neighbor contacts in the Fe K-edge EXAFS spectrum.

Experimental Section

Synthesis and General Characterization. $[DAP]_2[Fe_5(C_2O_4)_2(H_xPO_4)_8$, **I**, was prepared using hydrothermal techniques starting from 1,3-diaminopropane (DAP), $FeCl_3 \cdot 6H_2O$, $H_2C_2O_4$, and 85% (weight percent) ortho phosphoric acid. Starting materials were used as purchased from Sigma-Aldrich without further purification. To avoid photoreduction of Fe(III) by oxalate, the reaction was conducted in a dark room, with only a red-filtered light. In a typical synthesis 3.55 g of 85% H_3PO_4 (30 mmol) were diluted with 18 mL of deionized water, followed by the rapid addition of 0.763 g of 97% DAP (10 mmol). Addition of 1.35 g (5 mmol) of $FeCl_3 \cdot 6H_2O$ results in an amber colored solution which then turns to a pale green color upon addition of 0.630 g (5 mmol) of $H_2C_2O_4 \cdot 2H_2O$. The overall mole ratio of the reactants was 1:1:6:2:200 ($FeCl_3 \cdot 6H_2O/H_2C_2O_4 \cdot 2H_2O/H_3PO_4/DAP/H_2O$). The mixture was stirred for approximately 30 min and then transferred to a Parr acid digestion bomb, which was placed in an oven at 150 °C for 120 h. Upon cooling, crystalline solid products were isolated by filtration, then characterized by X-ray diffraction and thermogravimetric analysis.

Powder X-ray diffraction measurements were performed on samples loaded into 0.5 mm Pyrex capillaries affixed to a rotating goniometer on an INEL diffractometer using monochromatic Co radiation ($K_{\alpha 1}$ = 1.7890 Å) with a CPS-120 detector.

Thermogravimetric analysis (TGA) of **I** was carried out using a TA Instruments 2950 Thermogravimetric Analyzer in the temperature range 22−800 °C under a nitrogen atmosphere.

Single Crystal Structure. A single crystal of $[DAP]_2[Fe_5(C_2O_4)_2(H_xPO_4)_8$, **I**, was mounted on a nylon loop with a small amount of NVH immersion oil and affixed to a goniometer on a Bruker-Nonius X8 Apex2 diffractometer at a temperature of 173 K. Unit cell dimensions were determined from a symmetry constrained fit of 9933 reflections with $5.12° < 2\theta < 57.62°$. Reflections were collected from the entire Ewald sphere with 5002 unique reflections measured with a mixture of φ and ω scans collected up to 57.98° (2θ). The frame integration was performed using SAINT.[32] The resulting raw data were scaled, and the absorption was corrected using a multiscan averaging of symmetry equivalent data using SADABS.[33] The structure was solved by direct methods using the XS program.[34] All non-hydrogen atoms were obtained from the initial E-map. The hydrogen atoms for the 1,3-diammonium *n*-propyl cation were introduced at idealized positions and were allowed to ride on the parent atom. Attempts to find chemically reasonable atomic positions for hydrogens bonded to the PO_4 anions were unsuccessful and were therefore omitted from the final model. The structural model was fit to the data using full matrix least-squares based on an F of 4456 unique reflections [$I > 1.0\sigma(I)$]. The calculated structure factors included corrections for anomalous dispersion from the usual tabulation. The structure was refined using the LSTSQ program from NRCVAX.[35] The final R factors obtained were $R_f = 0.037$ and $R_w = 0.051$.

XAFS. X-ray absorption spectra were collected for standards and compound **I** on Beamline X-11B at the National Synchrotron Light Source (NSLS), Brookhaven National Laboratory. Iron foil, strengite ($FePO_4 \cdot 2H_2O$), and vivianite ($Fe_3(PO_4)_2 \cdot 8H_2O$) standards were purchased from a chemical supply company or synthesized according to literature procedures.[36] In a typical experiment, ~8 mg of sample were ground into fine powder and mixed with ~90 mg of boron nitride (BN) and then pressed into a 1.3 cm diameter plexiglass sample holder well of 1 mm depth. The storage ring was operating at a maximum current of 300 mA. Spectra were recorded in transmission mode using a channel-cut Si(111)-monochromator, which was detuned >30% to reject higher harmonics. The spectra were scanned in the range of 200 eV below to a wavevector (k) of 14 $Å^{-1}$ above the Fe K-edge at 7112 eV. All XANES spectra were normalized such that the edge step is 1.[37] Iron K-edge EXAFS data were processed using IFEFFIT package.[38,39] Data were k^2-weighted after being normalized for background removal in a k range of 0−13 $Å^{-1}$. Interatomic distances from a representative Fe atom (Fe2 was selected, being bound to both phosphate and oxalate) were calculated from crystallographic data of **I** using the ATOMS program inside the IFEFFIT package. Backscattering paths and phase corrections were calculated by the FEFF6 program. EXAFS data were Fourier transformed across a k range of 3.0−12.5 $Å^{-1}$ for an R-space fitting between 1.0 and 4.0 Å, which was conducted in the Artemis program. When fitting the data in Artemis, $k = 1$, $k = 2$, and $k = 3$ were chosen to optimize the fits over all three weighting factors.[37] When constructing the model, all paths with a computed amplitude of <20% were discarded because these paths were not needed to fit spectral features across the chosen k-space and R-space fitting ranges. To simplify the model, paths that are composed of the same atoms and whose difference of R_{eff} (from FEFF 6 calculation based on the crystal structure) is within 0.1 Å are grouped together. Normally, for each group of paths, the path whose R_{eff} is the closest to the R_{eff} average is included in the structure model to represent other paths. If all paths in that group have the same difference to the R_{eff} average, then the path with a higher amplitude is chosen. For each chosen path, the parameter coordination number (CN) is fixed as the combination of the degeneracy of all paths in that group, except for the Fe−O paths in the first coordination shell, due to its most dominant contribution to the overall EXAFS spectrum. In the structure of **I**, 2/3 Fe has both PO_4 and C_2O_4 coordinated, while 1/3 of Fe is only ligated to PO_4 such that out of the total of 18 Fe−O bonds to the 3 Fe metal centers, there are 4 $Fe-O_C$ bonds and 14 $Fe-O_P$ bonds. Thus the CN for $Fe-O_P$ path is fixed as 4.67, while it is 1.33 for the $Fe-O_C$ path. An amplitude reduction factor (So^2) of 0.84 was determined from EXAFS analysis of scorodite ($FeAsO_4 \cdot 2H_2O$) and was fixed in the theoretical model. When fitting the parameter "delR", an isotropic structural expansion factor "alpha" was introduced to all paths to allow a

(32) *SAINT*, version 7.34A; Bruker-Nonius: Madison, WI 53711, USA, 2006.
(33) *SADABS*, version 2.10; Bruker-Nonius: Madison, WI 53711, USA, 2004.
(34) *XS*, version 6.12; Bruker-AXS: Madsion, WI 53711, USA.
(35) Gabe, E. J.; Lepage, Y.; Charland, J. P.; Lee, F. L.; White, P. S. *J. Appl. Crystallogr.* **1989**, *22*, 384–387.
(36) Hesterberg, D.; Zhou, W. Q.; Hutchison, K. J.; Beauchemin, S.; Sayers, D. E. *J. Synchrotron Radiat.* **1999**, *6*, 636−638.
(37) Kelly, S.; Hesterberg, D.; Ravel, B., *Methods of Soil Analysis*; Soil Science Society of America: Madison, WI, 2008; pp 387−463.
(38) Newville, M. *J. Synchrotron. Radiat.* **2001**, *8*, 322–324.
(39) Ravel, B.; Newville, M. *J. Synchrotron Radiat.* **2005**, *12*, 537–541.

proportional (percentage) change in "delR" relative to "Reff" values that were calculated by the FEFF6 program.

Acknowledgment. This work was supported by the USDA-CSREES NRI Grant No. 2005-35107-16253 and NSF Grant No. DMR-0705190. Beamline X-11B (National Synchrotron Light Source - Brookhaven National Laboratory) is supported by DOE's Divisions of Materials Science and Chemical Sciences.

Supporting Information Available: Single crystal crystallographic information for $[DAP]_2[Fe_5(C_2O_4)_2(H_xPO_4)_8$, **I**, is available in .cif format. A figure of the TGA analysis of **I** is also provided in a supplemental figure. This material is available free of charge via the Internet at http://pubs.acs.org.

JA908807B